# Perfluorocyclobutane electronic state spectroscopy by high-resolution vacuum ultraviolet photoabsorption, electron impact, He I photoelectron spectroscopy, and *ab initio* calculations

P. Limão-Vieira,[1,2,*] E. Vasekova,[2] A. Giuliani,[3,4] J. M. C. Lourenço,[1] P. M. Santos,[5] D. Duflot,[6] S. V. Hoffmann,[7] N. J. Mason,[2] J. Delwiche,[3] and M.-J. Hubin-Franskin[3]

[1]*Laboratório de Colisões Atómicas e Moleculares, Departamento de Física, CEFITEC, Universidade Nova de Lisboa, P-2829-516 Caparica, Portugal*

[2]*Centre of Molecular and Optical Sciences, Department of Physics and Astronomy, The Open University, Walton Hall, Milton Keynes MK7 6AA, United Kingdom*

[3]*Laboratoire de Spectroscopie d'Électrons diffusés, Université de Liège, Institut de Chimie-Bât. B6c, B-4000 Liège 1, Belgium*

[4]*DISCO beamline, Synchrotron SOLEIL, BP 48, L'Orme des Merisiers, 91192 Gif-sur-Yvette CEDEX, France and Cepia, Institut National de la Recherche Agronomique, BP 71627, F-44316, Nantes, France*

[5]*Instituto de Telecomunicações, IST, Avenida Rovisco Pais, P-1049-001 Lisboa, Portugal*

[6]*Laboratoire de Physique des Lasers, Atomes et Molécules (PhLAM), UMR CNRS 8523, Centre d'Études et de Recherches Lasers et Applications CERLA, (CNRS 2416), Université des Sciences et Technologies de Lille, F-59655 Villeneuve d'Ascq Cedex, France*

[7]*Institute for Storage Ring Facilities, University of Aarhus, Ny Munkegade DK-8000, Århus C, Denmark*

The electronic state spectroscopy of perfluorocyclobutane ($c$-$C_4F_8$) has been investigated using high resolution vacuum ultraviolet (vuv) photoabsorption spectroscopy in the energy range 6.0–11 eV. The electron energy loss spectrum (EELS) was also recorded in the nonelectric dipolar interaction mode (100 eV incident energy, 10° scattering angle) over the 8–14 eV energy-loss range and the excited states in the 11–14 eV spectral region have been observed. An He I photoelectron spectrum recorded between 11.0 and 19.8 eV is compared with earlier lower resolution results. This has allowed us to derive a more precise value of 12.291±0.002 eV for the ground neutral state vertical ionization energy. All spectra presented in this paper represent the highest resolution data yet reported for perfluorocyclobutane, to the best of our knowledge. *Ab initio* calculations have been performed for helping in the assignment of the spectral bands for both neutral excited states and ionic states.

PACS number(s): 33.20.−t, 33.60.Cv, 33.70.Ca, 31.15.Ar

## I. INTRODUCTION

Perfluorocyclobutane, $c$-$C_4F_8$, is widely used for many diverse technologies from gaseous dielectric devices to retinal detachment surgery. Recently it has been used as a feed gas for $SiO_2$ reactive ion etching in the semiconductor industry being cited as a potential replacement of the traditional plasma processing molecules [1], e.g., $CF_4$, $SF_5CF_3$, and $SF_6$. However, $c$-$C_4F_8$ has a high global warming potential (GWP) of 8700 [2] and a long atmospheric lifetime depending on the sink mechanism in the upper atmosphere (the estimated lifetime due to photolysis and electron interactions being 1400 and 3200 years, respectively [2,3]). Determining the GWP and lifetime of any atmospheric molecule requires both knowledge of the electronic state spectroscopy and the absolute photoabsorption cross section in the visible and vacuum ultraviolet (vuv) region of the spectrum [4]. As part of a larger project to investigate the electronic state spectroscopy of several plasma processing molecules and to evaluate their role in global warming in the Earth's atmosphere, we have recorded a high-resolution vuv photoabsorption

spectrum of $c$-$C_4F_8$. As far as we are aware, no other spectra have been reported in the literature. These results are compared with an electron energy-loss spectrum.

In contrast to the paucity of data for photon absorption there have been several studies of electron interactions with $c$-$C_4F_8$. Christophorou and Olthoff [1] assembled a detailed compilation of recommended electron collision cross sections and transport-coefficient data for $c$-$C_4F_8$ that has been updated by (i) Winstead and McKoy [5], who calculated absolute cross sections for elastic and inelastic collisions of low-energy electrons using the Schwinger multichannel (SMC) method and (ii) experimentally derived absolute cross sections for elastic scattering and vibrational excitation by Jelisavcic *et al.* [6]. Miller *et al.* [7] have recently reported measurements on rate constants for electron attachment and thermal detachment to $c$-$C_4F_8$; they also performed Gaussian-3 second-order Moller-Plesset perturbation theory G3(MP2) and density-functional theory (DFT) calculations for ground state neutral geometry and information on efficiency of electron attachment. Energy-loss spectra in these experiments and excitation energies derived by theory are used to help assign the major bands in the photoabsorption spectra. Further information is derived from a high-resolution photoelectron spectrum which is used to identify the position of Rydberg states in the vuv spectrum.

The vuv absolute photoabsorption cross section spectrum has been used to derive the photolysis lifetime of $c$-$C_4F_8$ in the terrestrial atmosphere.

---

*Corresponding author. Present address: Laboratório de Colisões Atómicas e Moleculares, Departamento de Física, CEFITEC, Universidade Nova de Lisboa, P-2829-516 Caparica, Portugal. Fax: +351—21 294 85 49; plimaovieira@fct.unl.pt
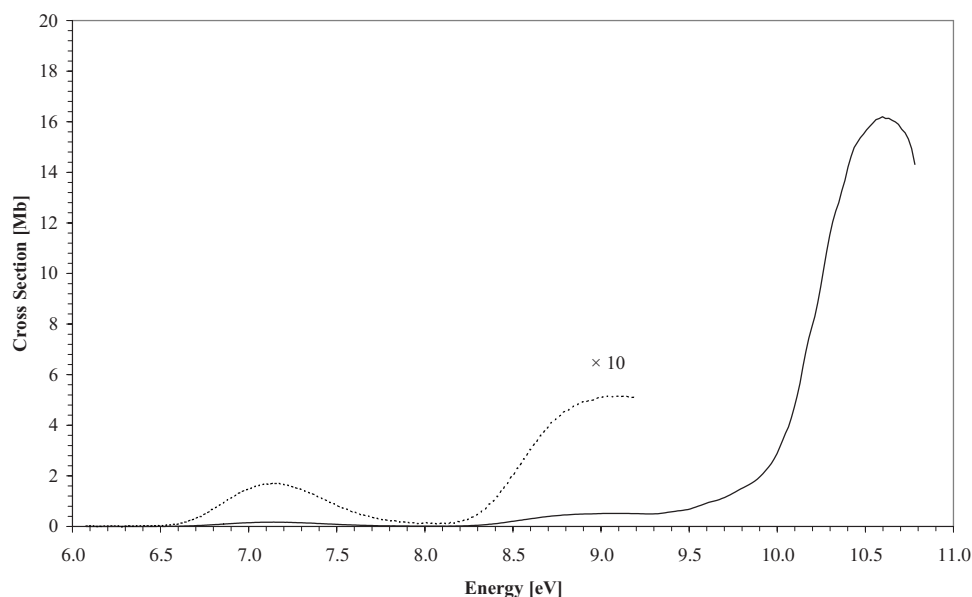
FIG. 1. High resolution vuv photoabsorption spectrum of $c$-$C_4F_8$ recorded using Aarhus synchrotron facility in the 6.0–10.8 eV energy range.

## II. EXPERIMENTAL SECTION

In order to study the spectroscopy of $c$-$C_4F_8$ we used a range of different techniques: vuv photoabsorption using a synchrotron source, which provides data on optical allowed transitions, high-resolution electron-energy-loss spectroscopy (HREELS), which allows forbidden as well as allowed transitions to be monitored, and photoelectron spectrum (PES) to determine the ionization energies.

### A. vuv photoabsorption

The present high-resolution vuv photoabsorption measurements (Figs. 1 and 2) were performed using the ASTRID-UV1 beam line at the Institute for Storage Ring Facilities (ISA), University of Aarhus, Denmark. A detailed description of the apparatus can be found elsewhere [8], so only a brief description will be given here. A toroidal dispersion grating is used to select the synchrotron radiation with a full width at half maximum (FWHM) wavelength resolution of approximately 0.075 nm. The synchrotron radiation passes through the gas sample stored in a gas cell maintained at room temperature. A photomultiplier is used to detect the transmitted light. For wavelengths below 200 nm a flow of He gas is flushed through the small gap between the photomultiplier and the exit window of the gas cell to prevent any absorption by air contributing to the spectrum. A LiF entrance window acts as an edge filter for higher order radiation restricting the photoabsorption measures to below 10.8 eV (115 nm). The grating itself provides a maximum wavelength (lower energy limit) of 320 nm (3.9 eV). The sample pressure is measured by a Baratron capacitance gauge. To avoid any saturation effects sample pressures were chosen such that the transmitted flux was >10% of the incident flux.

Gas transmission results are compared to a background scan recorded with an evacuated cell. Absolute photoabsorp-
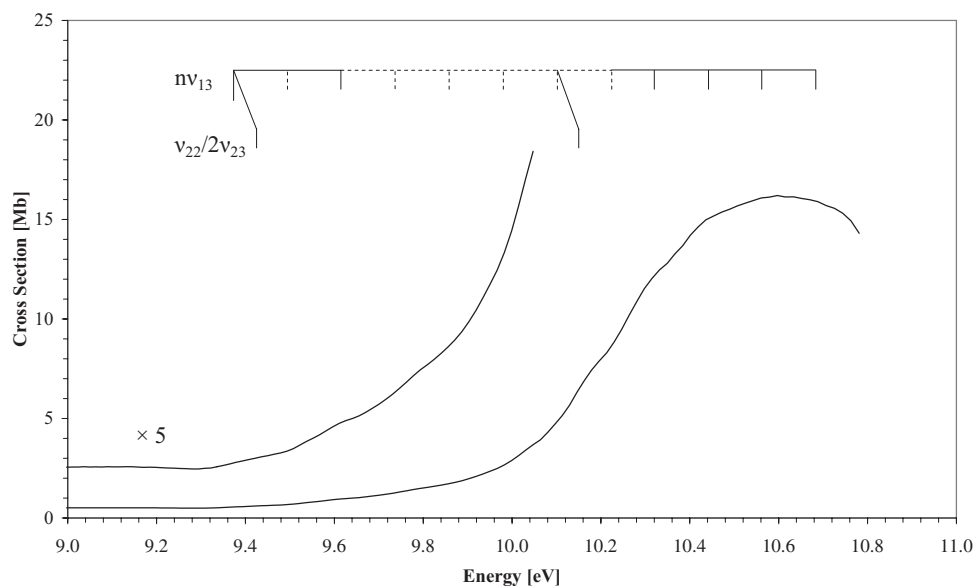


FIG. 2. High resolution vuv photoabsorption spectrum of $c$-$C_4F_8$ showing weak vibrational progressions in the 9.0–10.8 eV energy range.
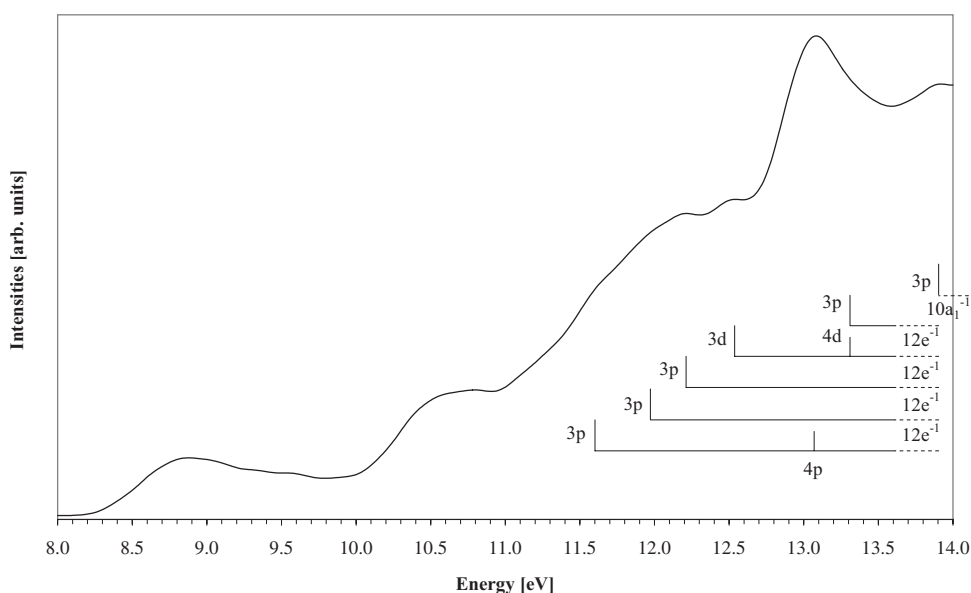
FIG. 3. Electron-energy-loss spectrum of $c$-$C_4F_8$ recorded at the University of Liège in the 8.0–14.0 eV energy region in the nonelectric dipolar interaction conditions (100 eV incident energy, 10° scattering angle).

tion cross sections may then be calculated using the Beer-Lambert law:

$$I_t = I_0 \exp(-n\sigma x),$$

where $I_t$ is the intensity of the light transmitted through the gas sample, $I_0$ is that through the evacuated cell, $n$ is the molecular number density of the sample gas, $\sigma$ is the absolute photoabsorption cross section, and $x$ is the absorption path length (25 cm). The accuracy of the absolute cross section is estimated to be better than ±5%.

### B. High-resolution electron-energy-loss spectroscopy

The instrument used at the Université de Liège, Belgium (VG-SEELS 400) has been described in detail elsewhere [9]. An electrostatic electron energy monochromator defines a narrow energy spread about the mean incident electron energy and a three element lens focuses the electrons into the collision region. The electron beam intersects the effusive gas beam, which flows through a hypodermic needle, at 90°. The working pressure is $\sim 1.5 \times 10^{-5}$ mbar. The analyzer system is also an electrostatic energy analyzer [9] with the scattered electron signal detected by an electron multiplier of the continuous dynode type. Both electron energy selectors work in the constant pass-energy mode. Spectra were recorded for energy losses between 8.0 and 14 eV at step intervals of 10 meV. The electron-energy-loss scale was calibrated to the "elastic scattering peak." The resolution, measured as the FWHM of the elastically scattered electron peak, was about 40 meV. The apparatus was used with relatively high incident energy electrons (100 eV) and a small scattering angle ($\theta = 10°$), such that nonelectric dipole interaction conditions apply. The present HREEL spectrum is shown in Fig. 3.

### C. Photoelectron spectroscopy

He I (21.22 eV) photoelectron spectra of $c$-$C_4F_8$ were recorded at the Université de Liège, Belgium (Fig. 4). The

experimental setup has been described in detail elsewhere [10]. Briefly, the spectrometer consists of a 180° hemispherical electrostatic analyzer with a mean radius of 5 cm. The analyzer is used in constant energy pass mode and is fitted with a continuous dynode electron multiplier. Incident photons are produced by a dc discharge in a two-stage differentially pumped lamp. The energy scale was calibrated using the $^2P_{3/2}$ (12.130 eV) and $^2P_{1/2}$ (13.436 eV) xenon peaks [11] for the low ionization energy part of the spectrum (up to 15.420 eV) and the $^2P_{3/2}$ (15.759 eV) and $^2P_{1/2}$ (15.937 eV) argon peaks [12] for the upper part. The spectra are corrected for the transmission function of the apparatus. The resolution of the present spectrum is measured from the FWHM of the Ar peaks to be 20 meV, in the presence of $c$-$C_4F_8$. The accuracy of the energy scale is estimated to be ±2 meV. The photoelectron spectrum presented in this paper is the sum of 20 individual spectra. This procedure allowed us to obtain a good signal-to-noise ratio while keeping the pressure in the spectrometer at a very low level ($<2 \times 10^{-6}$ mbar).

### D. Perfluorocyclobutane sample

The gas sample used in the vuv measurements was purchased from Fluorochem, with a minimum purity of 99%, while for photoelectron spectroscopy (PES) and HREELS experiments the sample was purchased from ABCR with a quoted 99% purity.

### III. COMPUTATIONAL SECTION

To complement and help to interpret our experimental results, we performed *ab initio* calculations to determine vertical excitation energies of the electronic states and the lowest ionization energies.

It is well known that the calculation of electronic spectra, even for small organic molecules, is a difficult task (see Ref. [13] for a recent review). Because of its low computational cost, the time-dependent density-functional theory (TDDFT) method has recently become a very popular method [14] and
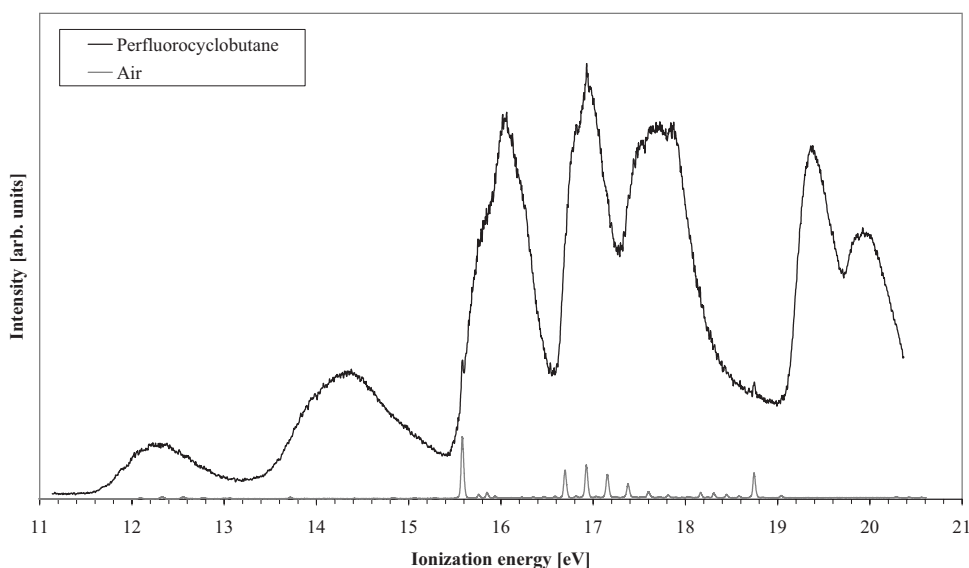
FIG. 4. He I photoelectron spectra of $c$-$C_4F_8$ and air which is present as a contaminant in very small amounts (see text), recorded at the University of Liège.

in the case of the acrolein molecule, the PBE0 functional of [15,16] was shown to give results in good agreement with more costly calculations [i.e., multiple scattering-complete-active-space second-order perturbation theory (MS-CASPT2]. Therefore, the same method was employed in the present work: the geometry was optimized at the DFT/PBE0/6–311G$^{**}$ level (Table I) and the electronic excitation spectrum was calculated at the TDDFT//PBE0/6–311++G$^{**}$ level (Table II). These calculations were performed with the GAUSSIAN 03 package [17]. However, it is also well known [13,14] that TDDFT presents problems with the description of certain types of electronic states, including Rydberg states. Thus, the lowest lying excited states were also computed at the CCS, CC2 [18], and CCSD [19] levels (second-order approximate coupled cluster single, double and single and double excitations level, respectively) with the DALTON program [20] (Table III). The geometry was optimized at the second-order Moller-Plesset correlation-consistent polarization valence double $\zeta$ (MP2 cc-pVDZ) level and then diffuse functions $(5s,5p,5d)$ taken

from Kaufmann *et al.* [21] were added at the center of the molecule (cc-pVDZ+$R$ basis set). These calculations were performed in the $C_{2v}$ group, which is the largest Abelian subgroup of $D_{2d}$. Finally, the lowest ionization energies of $c$-$C_4F_8$ were obtained with the same geometry and basis set (Table IV) at the RCCSD {single-configuration [spin restricted (R)] coupled-cluster approach including single and double} [22], RCCSD(T) {single-configuration [spin restricted (R)] coupled-cluster approach including single and double and a perturbative estimate of triple excitations} [23], and MR-AQCC (multireference averaged quadratic coupled cluster) [24] levels, using the MOLPRO package [25]. For the MR-AQCC calculations, the reference space was limited to the ROHF (restricted open Hartree-Fock) determinant of the first ionic state of each symmetry.

## IV. RESULTS AND DISCUSSION

### A. Structure and properties of $c$-$C_4F_8$

The calculated geometry is shown in Fig. 5(a) and the corresponding parameters are listed in Table I. Using this

TABLE I. Calculated geometry of $c$-$C_4F_8$ compared with previous works (bond lengths in Å and angles in degrees).

| | Cation ($^2B_1$) PBE0[a] 6−311 G$^{**}$ | Ground state PBE0[a] 6−311 G$^{**}$ | MP2[a] cc-pVDZ | G3(MP2)[b] | B3LYP[c] 6−31 G$^*$ | MP2[c] 6−31 G$^*$ | Experiment[d] | Anion ($^2A_u$) G3(MP2)[b] |
|---|---|---|---|---|---|---|---|---|
| C-C | 1.6398 | 1.5611 | 1.5587 | 1.550 | 1.566 | 1.552 | 1.566±0.008 | 1.489 |
| C-$F_1$ | 1.2973 | 1.3345 | 1.3462 | 1.350 | 1.346 | 1.353 | 1.333±0.002 | 1.489 |
| C-$F_2$ | 1.2901 | 1.3287 | 1.3367 | 1.340 | 1.340 | 1.342 | 1.333±0.002 | 1.489 |
| CCC | 88.1 | 89.4 | 88.5 | | 89.4 | 88.6 | 89.3±0.3 | |
| $F_1$CC | 111.4 | 112.2 | 111.3 | | 112.1 | 110.9 | | |
| $F_2$CC | 115.4 | 115.7 | 116.8 | | 115.5 | 116.9 | | |
| $F_1$C$F_2$ | 113.0 | 110.4 | 110.6 | | 110.7 | 111.0 | 109.9±0.3 | |
| CCCC | 20.7 | 12.0 | 18.2 | 17.1 | 10.5 | 17.7 | 17.4 | |

[a]This work.
[b]Reference [7].
[c]Reference [27].
[d]Reference [34].

TABLE II. Calculated vertical excitation energies (TDDFT/PBE0/6−311++G$^{**}$//PBE0/6−311 G$^{**}$) of $c$-C$_4$F$_8$ (eV) and oscillator strengths of the lowest lying states.

| Symmetry | Energy[a] (eV) | $f$ | Main character | Experiment[b] (eV) |
|---|---|---|---|---|
| $^1A_2$ | 6.695 | — | $3b_1 \rightarrow \sigma^*$(C-F)/$\pi$(C-C)$(b_2)$ | 7.142 |
| $^1B_1$ | 8.404 | — | $3b_1 \rightarrow 3s(a_1)$ | 9.143 |
| $^1E$ | 8.597 | 0.0005 | $12e \rightarrow 3p(e)$ | — |
| $^1E$ | 9.717 | 0.0007 | $3b_1 \rightarrow 3p(e)$ | — |
| $^1B_2$ | 9.992 | 0.0008 | $10a_1 \rightarrow \sigma^*$(C-F)/$\pi$(C-C)$(b_2)$ | — |
| $^1E$ | 10.065 | 0.0176 | $12e \rightarrow 3s(a_1)$ | — |
| $^1E$ | 10.104 | 0.0311 | $11e \rightarrow \sigma^*$(C-F)/$\pi$(C-C)$(b_2)$ | 10.597 |
| $^1A_2$ | 10.275 | — | $2b_1 \rightarrow \sigma^*$(C-F)/$3p\pi(b_2)$ | — |
| $^1A_2$ | 10.509 | — | $3b_1 \rightarrow 3p\pi(b_2)$ | — |
| $^1A_1$ | 10.676 | — | $9b_2 \rightarrow \sigma^*$(C-F)/$\pi$(C-C)$(b_2)$ | — |
| $^1A_2$ | 10.885 | — | $3b_1 \rightarrow 3d(b_2)$ | — |
| $^1E$ | 10.892 | 0.0049 | $10e \rightarrow \sigma^*$(C-F)/$\pi$(C-C)$(b_2)$ | 10.597 |
| $^1E$ | 10.970 | 0.0014 | $3b_1 \rightarrow 3d(e)$ | 10.597 |
| $^1A_1$ | 10.970 | — | $3b_1 \rightarrow 3d(b_1)$ | — |
| $^1B_1$ | 10.987 | — | $3b_1 \rightarrow 3d(a_1)$ | — |
| $^1B_2$ | 11.267 | 0.0357 | $9a_1 \rightarrow \sigma^*$(C-F)/$\pi$(C-C)$(b_2)$ | — |
| $^1B_1$ | 11.277 | — | $1a_2 \rightarrow \sigma^*$(C-F)/$\pi$(C-C)$(b_2)$ | — |
|  |  |  | $+2a_2 \rightarrow \sigma^*$(C-F)/$\pi$(C-C)$(b_2)$ | — |
| $^1A_1$ | 11.335 | — | $10a_1 \rightarrow 3s(a_1)$ | — |
| $^1B_1$ | 11.347 | — | $1a_2 \rightarrow \sigma^*$(C-F)/$\pi$(C-C)$(b_2)$ | — |
|  |  |  | $+2a_2 \rightarrow \sigma^*$(C-F)/$\pi$(C-C)$(b_2)$ | — |
| $^1A_1$ | 11.394 | — | $12e \rightarrow 3p(e)$ | — |
|  |  |  | $+3b_1 \rightarrow 4s(a_1)$ | — |
| $^1A_2$ | 11.414 | — | $12e \rightarrow 3p(e)$ | — |
| $^1B_2$ | 11.420 | 0.0024 | $12e \rightarrow 3p(e)$ | — |
| $^1E$ | 11.477 | <0.0001 | $11e \rightarrow 3s(a_1)$ | — |
| $^1B_1$ | 11.478 | — | $12e \rightarrow 3p(e)$ | — |
| $^1B_1$ | 11.486 | — | $3b_1 \rightarrow 4p(e)$ | — |
|  |  |  | $+12e \rightarrow 3p(e)$ | — |
| $^1E$ | 11.530 | 0.1439 | $3b_1 \rightarrow 4p(e)$ | — |
| Ion[a] ($^2B_1$) | 11.653 | — | — | — |

[a]PBE0/6−311 G$^{**}$ value.
[b]This work.

geometry, the calculated electron configuration of the $\widetilde{X}\ ^1A_1$ ground state of $c$-C$_4$F$_8$ is

(a) core 1$s$ orbitals $1a_1^2\ 1e^4\ 1b_2^2\ 2b_2^2\ 2e^4\ 2a_1^2\ 3a_1^2\ 3e^4\ 3b_2^2$;

(b) $\sigma$(C-F) orbitals $4a_1^2\ 4e^4\ 4b_2^2\ 5b_2^2\ 5e^4\ 5a_1^2$;

(c) $\sigma$(CC) orbitals $6a_1^2\ 6e^4\ 6b_2^2$;

(d) $p$(F) lone pairs $7a_1^2\ 7b_2^2\ 1b_1^2\ 7e^4\ 8e^4\ 8a_1^2\ 9e^4\ 8b_2^2$ $1a_2^2\ 2a_2^2\ 9a_1^2\ 10e^4\ 9b_2^2\ 2b_1^2\ 11e^4\ 10a_1^2\ 12e^4$;

(e) $\sigma$(C-C)/$p$(F) lone pair $3b_1^2$.

The highest occupied molecular orbital (HOMO) in the neutral ground state is localized on the fluorine lone pair electrons with $\sigma$(C-C)/$n_F(3b_1)$ mixing character as shown in Fig. 5(b), using the MOLDEN software [26].

The lowest unoccupied molecular orbital (LUMO) is the $\sigma^*$[C-F(10$b_2$)] orbital, with a slightly $\pi$(C-C) bonding character [Fig. 5(c)]. A few vertical ionization energy values for $c$-C$_4$F$_8$ have been reported by Christophorou and Olthoff [1]

for the $3b_1^{-1}$ orbital in reasonable agreement with our present high-resolution He I photoelectron spectrum (see Sec. IV E). Excitation of a $3b_1$ electron may also lead to Rydberg state members of series converging to the ionic ground electronic state.

The ground state geometry calculated with the two methods (PBE0 and MP2) is compared with previous works in Table I. Bond lengths at PBE0 level are in better agreement with experiment than MP2 values. On the other hand, the MP2 ring-puckering angle [see Fig. 5(a)] of 18.2° is closer to experiment (17.4°) than the PBE0 result of 12.0°. The first column of Table I shows the optimized geometry of the first cationic state ($3b_1^{-1}$ ionization). The increase of C-C bond length when compared to the neutral molecule is consistent with the C-C bonding nature of the HOMO as displayed in Fig. 5: removal of an electron from the HOMO weakens the

TABLE III. (a) Calculated vertical excitation energies (CC/cc-pVDZ+R//MP2/cc-pVDZ) of $c$-$C_4F_8$ (eV), oscillator strengths of the lowest lying states and present experimental vuv and EELS data (see discussion in text); (b) tentative assignments for the 11–14 eV EELS band.

(a)

| | CCS E (eV) | $f_L$ | CC2[a] E (eV) | $f_L$ | CCSD[a] E (eV) | $f_L$ | Main character[a,b] | Experiment[a] vuv | (eV) EELS |
|---|---|---|---|---|---|---|---|---|---|
| $^1A_2$ | 9.09 | — | 7.37 | — | 7.73 | — | $3b_1 \rightarrow \sigma^*(\text{C-F})/\pi(\text{C-C})(b_2)$ | 7.142 | — |
| — | — | — | — | — | — | — | — | — | 8.880 |
| $^1B_1$ | 10.94 | — | 8.54 | — | 9.04 | — | $3b_1 \rightarrow 3s(a_1)$ | 9.143 | 9.000 |
| $^1E$ | 11.43 | 0.0030 | 9.49 | 0.0010 | 9.87 | 0.0008 | $3b_1 \rightarrow \sigma^*(\text{C-F})/\pi(\text{C-C})(b_2)$ | — | 9.520 |
| $^1E$ | 11.88 | <0.0001 | 9.40 | 0.0052 | 9.98 | 0.0033 | $3b_1 \rightarrow 3p(e)$ | — | 9.520 |
| $^1A_2$ | 12.19 | — | 9.62 | — | 10.24 | — | $3b_1 \rightarrow 3p\,\pi(b_2)$ | — | — |
| $^1B_1$ | 12.42 | — | 9.94 | — | 10.57 | — | $3b_1 \rightarrow 3d(a_1)$ | — | — |
| $^1A_1$ | 12.56 | <0.0001 | 10.01 | <0.0001 | 10.66 | <0.0001 | $3b_1 \rightarrow 3d(b_1)$ | 10.597 | 10.780 |
| $^1A_2$ | 12.63 | — | 10.05 | — | 10.71 | — | $3b_1 \rightarrow 3d(b_2)$ | — | — |
| $^1E$ | 12.68 | 0.0005 | 10.08 | <0.0001 | 10.74 | <0.0001 | $3b_1 \rightarrow 3d(e)$ | — | — |
| $^1E$ | 12.80 | 0.0466 | 10.29 | 0.0025 | 10.87 | 0.0223 | $12e \rightarrow 4s(a_1)+3b_1 \rightarrow 4p(e)$ | 10.597 | 10.780 |

(b)

| This work EELS (eV) | Tentative assignment | Ionization energy limit (eV) | Quantum defect |
|---|---|---|---|
| 11.300 | — | — | — |
| 11.660 | $3p$ | 14.336 | 0.75 |
| 11.980 | $3p$ | 14.336 | 0.60 |
| 12.220 | $3p$ | 14.336 | 0.47 |
| 12.540 | $3d$ | 14.336 | 0.25 |
| 13.080 | $4p$ | 14.336 | 0.71 |
| 13.320 | $4d/3p$ | 14.336/16.055 | 0.34/0.77 |
| 13.920 | $3p$ | 16.055 | 0.48 |

[a]This work.
[b]From CCS wave functions.

C-C bond and increases its bond length. It is also interesting to compare the ground state geometry with that of the anion molecule $c$-$C_4F_8^-$, calculated by Miller *et al.* [7], which has the peculiarity of having a planar carbon ring and symmetry ($D_{4h}$) higher than the neutral species. The lengthening of the C-F bonds and shortening of the C-C bonds in the anion with respect to the neutral is fully consistent with the $\sigma^*(\text{C-F})$ and $\pi(\text{C-C})$ character of the LUMO.

TABLE IV. Calculated and experimental He I photoelectron ionization energies of $c$-$C_4F_8$ (values in eV).

| Configuration | RCCSD[a] | RCCSD(T)[a] | MR-AQCC[a] | OVGF[b] | Experiment[a] |
|---|---|---|---|---|---|
| $3b_1^{-1}$ | 12.086 | 11.763 | 12.123 | 12.1 | 12.291 |
| $12e^{-1}$ | 14.047 | 13.687 | 14.016 | 14.0 | 14.336 |
| $11e^{-1}$ | | | 15.979 | | 16.055 |
| $10a_1^{-1}$ | 16.237 | 15.628 | 15.986 | | 16.055 |
| $2b_1^{-1}$ | | | 16.572 | | 16.946 |
| $9b_2^{-1}$ | | | 16.594 | | 16.946 |
| $10e^{-1}$ | | | 16.923 | | 16.946 |
| $2a_2^{-1}$ | | | 17.345 | | 17.524/17.692 |
| $9e^{-1}$ | | | 17.600 | | 17.692/17.848 |
| $8e^{-1}$ | | | 19.914 | | 19.932 |

[a]This work.
[b]Reference [30]. Values obtained at the MP2/6−311 G+($d$,$p$) geometry.
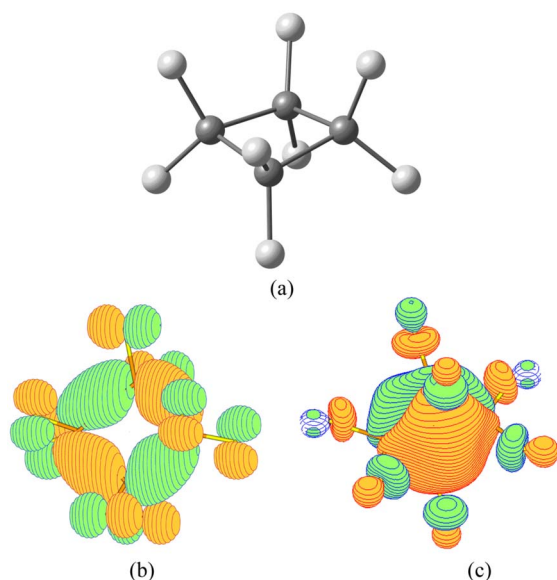
FIG. 5. (Color online) (a) Ground-state structure of $c$-$C_4F_8$; (b) highest occupied molecular orbital (HOMO) of $c$-$C_4F_8$; (c) lowest unoccupied molecular orbital (LUMO) of $c$-$C_4F_8$.

In its ground neutral electronic state $c$-$C_4F_8$ has $D_{2d}$ symmetry, with 23 modes of vibration [6]. In the present high-resolution absorption spectrum, very weak vibrational modes with mean excitation energies of 0.120 and 0.046 eV were observed. Comparing these values with vibrational energies of the ground state [27], these have been tentatively assigned (Table V) by comparison with the unfluorinated analog $c$-$C_4H_8$ [28], to the $\nu_{13}(b_2)$ $CF_2$ symmetric stretching (0.152 eV) and the $\nu_{22}(e)$ $CF_2$ wagging (0.055 eV) or $2\nu_{23}(e)$ ring deformation (0.048 eV) modes, respectively.

The calculated transition energies, oscillator strengths, and the main character of the wave function are shown in Tables II (TDDFT results) and III (CC results). Due to the high symmetry of the molecule, many transitions are electric-dipole forbidden. The comparison between the two tables shows several patterns which are well known in the calculations of electronic spectra [13,14]: the CCS (or CIS) values give too large energies and this method has no quantitative accuracy. There are also differences of several tenths of an eV between TDDFT and both CC values and it seems that the CCSD values are larger than CC2 by about 0.5 eV. Except for transitions to the LUMO, which has valence character, the TDDFT method is expected to give overestimated results for Rydberg transitions. A possible hierarchy of the

TABLE V. Calculated vibrational energies for both ground and lowest ionic states of $c$-$C_4F_8$ (energies in eV).

| $D_{2d}$ species | Calculation: neutral ground state[a] | Experiment[b] (IR spectroscopy) | Experiment[b] (Raman spectroscopy) | Calculation: ionic ground state[a] |
|---|---|---|---|---|
| $a_1$ | 0.182 | — | 0.178 | 0.178 |
| | 0.162 | — | 0.175 | 0.172 |
| | 0.089 | — | 0.087 | 0.090 |
| | 0.076 | — | 0.075 | 0.071 |
| | 0.046 | — | 0.045 | 0.044 |
| | 0.005 | — | — | 0.007 |
| $a_2$ | 0.110 | — | — | 0.102 |
| | 0.027 | — | — | 0.025 |
| $b_1$ | 0.127 | — | 0.125 | 0.118 |
| | 0.034 | — | 0.032 | 0.032 |
| | 0.032 | — | — | 0.028 |
| $b_2$ | 0.162 | 0.160 | 0.160 | 0.174 |
| | 0.157 | 0.152 | 0.152 | 0.161 |
| | 0.083 | 0.082 | 0.082 | 0.084 |
| | 0.043 | 0.043 | 0.044 | 0.044 |
| | 0.024 | 0.035 | — | 0.022 |
| $e$ | 0.169 | 0.166 | 0.166 | 0.169 |
| | 0.155 | 0.154 | — | 0.145 |
| | 0.122 | 0.119 | — | 0.078 |
| | 0.071 | 0.071 | — | 0.055 |
| | 0.055 | 0.055 | 0.054 | 0.037 |
| | 0.035 | — | 0.034 | 0.031 |
| | 0.023 | 0.024 | 0.024 | 0.017 |

[a]This work (PBE0/6−311 G$^{**}$).
[b]Reference [28].

TABLE VI. Vibrational assignments in the 9.0–11.0 eV absorption band of $c$-$C_4F_8$. Assignment within brackets (?) means uncertainty; (d) means diffuse structure.

| This work Energy (eV) | Assignment | $\Delta E(\nu_{13})$ (eV) | $\Delta E(\nu_{21}/2\ \nu_{23})$ (eV) |
|---|---|---|---|
| 9.372 | $\nu_{00}$ | — | — |
| 9.421 | $1\nu_{22}/1\nu_{23}$ | — | 0.049 |
| 9.493 (d) | $1\nu_{13}(?)$ | — | — |
| 9.611 | $2\nu_{13}$ | 0.118 | — |
| 9.740 (d) | $3\nu_{13}(?)$ | — | — |
| 9.856 (d) | $4\nu_{13}(?)$ | — | — |
| 9.983 (d) | $5\nu_{13}(?)$ | — | — |
| 10.104 (d) | $6\nu_{13}(?)$ | — | — |
| 10.146 | $6\nu_{13}+1\nu_{22}/1\nu_{23}$ | — | 0.042 |
| 10.213 (d) | $7\nu_{13}(?)$ | — | — |
| 10.315 | $8\nu_{13}$ | 0.102 | — |
| 10.436 | $9\nu_{13}$ | 0.121 | — |
| 10.561 | $10\nu_{13}$ | 0.125 | — |
| 10.688 | $11\nu_{13}$ | 0.127 | — |

present calculations could thus be $CCS < TDDFT < CC_2 < CCSD$.

## B. Neutral excited states

The high-resolution absolute vuv photoabsorption spectrum of perfluorocyclobutane recorded between 6.0 and 11.0 eV using the Aarhus synchrotron facility is shown in Figs. 1 and 2.

Three absorption bands centered at 7.142, 9.143, and 10.597 eV may be identified as transitions from the $\tilde{X}\ ^1A_1$ neutral ground state to the $^2A_1$, $^1B_1$, and $^1A_1$ states, respectively (Tables II and III). All bands are quite broad (Fig. 1) suggesting rapid dissociation into neutral radicals with only diffuse, not very well resolved, structure being observed in the latter (Table VI) and reported here. The transitions involved for each band have been assigned to $10b_2$: $^1A_2 \leftarrow 3b_1$: $\tilde{X}\ ^1A_1$ [5], $3s \leftarrow 3b_1(^1B_1 \leftarrow \tilde{X}\ ^1A_1)$, and $3d \leftarrow 3b_1(^1A_1 \leftarrow \tilde{X}\ ^1A_1)$, respectively (Table III). Following the assignment proposed by Winstead and McKoy [5] for the first, weak absorption feature, it was attributed to the excitation of an electron from the HOMO centered on the fluorine lone pair ($n$) to the LUMO of C-F($10b_2$) $\sigma^*$ antibonding character. A transition into the singlet $A_2$ state is symmetry disfavored by the forbidden dipole-electric transition and reinforced by the very weak magnitude observed in the present spectra (the local maximum cross sectional value is 0.171 Mb). However, and due to the fact that $c$-$C_4F_8$ shows two reflection planes containing the symmetry axis, the forward and backward excitation cross sections in the electron interaction are reduced but not entirely suppressed as stated in Ref. [5]. Symmetry disfavored by forbidden dipole-electric transitions is also remarkable for the $B_1$ state with a low cross sectional value of 0.515 Mb. The present calculations, reported in Tables II and

III, for the two lowest absorption bands are in good agreement with the assignments proposed previously. As far as the assignment of the third band is concerned, the calculations show a mixing of several Rydberg transitions ($3p, 3d, \ldots$). However, and due to the broad nature of this band, a predictable transition to a $\sigma^*$(C-F) antibonding orbital with a high oscillator strength value may be possible (Table II).

## C. Vibrational excitation in the energy range 9.0–11.0 eV

The vuv spectrum in this energy region is a broad continuum (Figs. 1 and 2) with two maxima lying at 9.143 eV (0.515 Mb) and 10.597 eV (16.201 Mb), respectively. However superimposed upon these is a weak structure which may be ascribed to Rydberg character (see Rydberg series section). The band also exhibits an extended poorly defined progression which may be ascribed to the $CF_2$ symmetric stretching, $\nu_{13}(b_2)$ and the $CF_2$ wagging, $\nu_{22}(e)$ or ring deformation, $2\nu_{23}(e)$ modes (Table VI). Recently, for the neutral ground state, Jelisavcic *et al.* [6] have observed by electron impact that due to the limited resolution (50 meV) available in their experiments, most of the low-energy modes could not be resolved from the elastic peak as well as some of the high-energy modes and their overtones. However, the $\sim$120 meV structure observed ($\Delta\nu_{13}$) is reinforced by the IR presence at $\sim$120 and 157 meV, which we also report in the calculation results of Table V (0.161 eV). Due to the difficulty in assigning a vibrational mode to the mean excitation energy of 0.046 eV, we have decided to label the weak excitation series starting at 9.421 eV as $\nu_{22}/2\nu_{23}$. $\Delta\nu_{22}$ and $\Delta 2\nu_{23}$ are almost in the ratio 1:2, and therefore the normal mode description of vibrations for the lowest lying excitations may be related to possible strong Fermi resonance.

## D. Rydberg series

The cross section above 9 eV consists of two large maxima assigned also to Rydberg structure progressing up to the lowest ionization limit, 12.291 eV (Fig. 3). The peak positions, $E_n$, must fit the Rydberg formula: $E_n = E_i - R/(n - \delta)^2$, where $E_i$ is the ionization energy, $n$ is the principal quantum number of the Rydberg orbital of energy $E_n$, $R$ is one Rydberg, and $\delta$ is the quantum defect resulting from the penetration of the Rydberg orbital into the core. The two bands at 9.143 and 10.597 eV (Fig. 1) have been identified to correspond to the $3s \leftarrow 3b_1(^1B_1 \leftarrow \tilde{X}\ ^1A_1)$ and $3d \leftarrow 1b_1(^1A_1 \leftarrow \tilde{X}\ ^1A_1)$ Rydberg transitions, with quantum defects $\delta$ of 0.92 and 0.17, respectively. A comparison of the calculated vertical excitation energies in Table III with the present vuv photoabsorption and electron-energy-loss (EEL) features shows some tentative assignments for the structure observed. The electron-energy-loss weak shoulder feature at 11.300 eV remains unassigned. The relative intensity of the spectral bands in the EEL spectrum is different from those in the optical absorption due to the fact that symmetry forbidden transitions are expected to be excited in interaction conditions prevailing in the EEL spectrum.
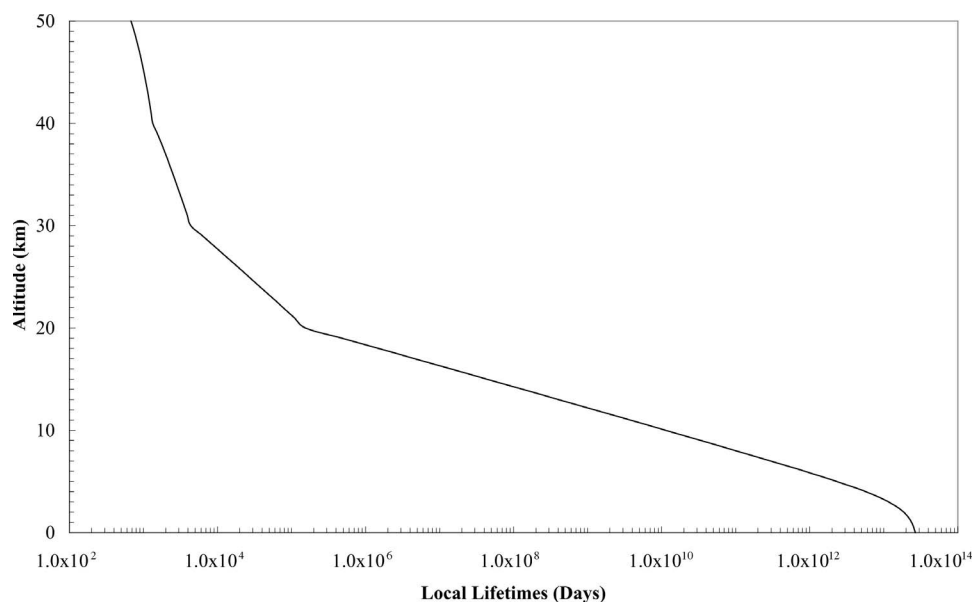
FIG. 6. The local lifetime of perfluorocyclobutane between 0 and 50 km obtained from its vuv photoabsorption spectrum shown in Fig. 1.

### E. Ionic states

Figure 4 shows the bands associated with the ionic states of $c$-$C_4F_8$. The sample contains a small contamination of air, but this does not affect the assignment of the $c$-$C_4F_8$ features since the narrow lines due to $N_2$ can be readily identified. Since there is no vibrational structure associated with the ionic states, the contamination does not affect our assignment of the weak vibrational pattern observed in the vuv spectra or the ionization energy limits for the assigned Rydberg series. The energy positions of the observed features are summarized in Table IV. The shape of the observed lowest ionic band for $c$-$C_4F_8^+$ (Fig. 4) is quite broad and structureless, the maximum intensity at $(12.291 \pm 0.002)$ eV corresponds to the vertical ionization energy. The onset of ionization is measured at $(11.60 \pm 0.05)$ eV in good agreement with the value determined by Jarvis *et al.* [29] and Parkes *et al.* [30] in their study of perfluorocyclobutane by the threshold photoelectron-photoion coincidence method. Photoelectron spectroscopy gives both the adiabatic (a very probable value) and vertical ionization energies, the values of which tend to differ significantly whenever there is a large change in equilibrium molecular geometry on ionization [12]. The absence of vibrational structure in the first electronic band of the photoelectron spectrum is due to the very fast decomposition of the $c$-$C_4F_8$+molecular producing $C_3F_5^+$+$CF_3$ as shown by Jarvis *et al.* [29] and Parkes *et al.* [30].

The results of the present calculations, shown in Table IV, agree very well with the experimental values obtained for the electronic bands of the photoelectron spectrum, especially for the AQCC method and contrary to the CCSD(T) energies which were found to be too low. Moreover, the TDDFT/PBE0 value of 11.653 eV (Table II) is also underestimated. According to Table IV, the first band is unambiguously assigned to the $3b_1^{-1}$ state and the second band to the $12e^{-1}$ state. The asymmetry of the third band, which can be clearly seen in Fig. 4 is due to the presence of two nearly degenerate ionic states ($11e^{-1}$ and $10a_1^{-1}$) in this region. At higher energies, the situation is less clear because of the large number of

states, as shown in Table IV. It should be noted that due to convergence problems, it was not possible to calculate higher lying $A_1$ states with the MR-AQCC method. The high density of ionic states may be connected to the fact that the highest occupied MO's in $c$-$C_4F_8$ are essentially lone pairs with very similar energies. The present results are consistent with the outer valence Green's function (OVGF) calculations of Parkes *et al.* [30] (see Fig. 4 in Ref. [30]), although these authors only provide the first two ionization energies. The absence of structures at 12.8 and 14.8 eV in the present photoelectron spectrum (PES) is explained by the fact that these structures observed in the threshold photoelectron spectroscopy (TPES) spectrum [30] of $c$-$C_4F_8$ are due to Rydberg states that autoionize, as already suggested by Parkes *et al.* These authors report that at that time there was no PES available the present results fulfill that gap and support their predictions.

### V. PHOTOLYSIS RATES AND LOCAL LIFETIMES

The present cross section values can be used to model the atmospheric destruction of $c$-$C_4F_8$ by uv photolysis as a function of altitude. Details of the program are presented in a previous publication by Limão-Vieira *et al.* [31]. Photolysis rates at a given wavelength were calculated as the product of the solar actinic flux [32] and the molecular photoabsorption cross section at 1 km altitude steps from the surface up to the stratopause (50 km). At each altitude a total photolysis rate may then be calculated by summing over the individual photolysis rates for that altitude. The reciprocal of the total photolysis rate for a given altitude gives the local photolysis lifetime at that altitude, i.e., the time taken for the molecule to photodissociate at the altitude assuming that the solar flux remains constant. The local lifetimes shown in Fig. 6 assume that the quantum yield for dissociation is unity. The results show that the local photolysis lifetime of $c$-$C_4F_8$ varies from about 400 years at 20 km to a few days at 40–50 km. Therefore, it indicates that perfluorocyclobutane will be stable to

photolysis in the troposphere but can be broken up reasonably at higher altitudes. We have recently reported a high-resolution Fourier transform infrared (FTIR) spectra [33] showing a strong infrared absorption cross section in the wavelength region of the Earth's atmospheric window $(800-1300 \text{ cm}^{-1})$, such that a long tropospheric lifetime may lead to significant global warming potential of 8500 times that of $CO_2$. However, the atmospheric lifetime of $c\text{-}C_4F_8$ can be significantly reduced by electron interactions, according to Morris *et al.* [3].

## VI. CONCLUSIONS

The present results are experimental data on the spectroscopy of perfluorocyclobutane in the 6.0–11.0 eV energy region. In the high-resolution data features are observed. Weak fine structure observed in the 9 eV photoabsorption band has been assigned to specific vibrational modes.

*Ab initio* calculations on the vertical excitation energies and oscillator strengths were used in the assignment of the spectral transitions. The theoretical results are in good agreement with the experimental data for both neutral excited states and ionic states.

The measured photoabsorption cross sections have been used to derive the local lifetime in the Earth's atmosphere

$(0-50 \text{ km})$ showing that perfluorocyclobutane may have a long residence time in the lower atmosphere.

[1] L. G. Christophorou and J. K. Olthoff, J. Phys. Chem. Ref. Data **30**, 449 (2001).

[2] J. T. Houghton, L. G. M. Filho, B. A. Callander, N. Harris, A. Kattenberg, and K. Maskell, *Climate Change 1995* (Cambridge University Press, New York, 1996).

[3] R. A. Morris, T. M. Miller, A. A. Viaggiano, J. F. Paulson, S. Solomon, and G. Reid, J. Geophys. Res. **100**, 1287 (1995).

[4] N. J. Mason, A. Dawes, R. Mukerji, E. A. Drage, E. Vasekova, S. M. Webb, and P. Limão-Vieira, J. Phys. B **38**, S893 (2005).

[5] C. Winstead and V. McKoy, J. Chem. Phys. **114**, 7407 (2001).

[6] M. Jelisavcic, R. Panajotovic, M. Kitajima, M. Hoshino, H. Tanaka, and S. J. Buckman, J. Chem. Phys. **121**, 5272 (2004).

[7] T. M. Miller, J. F. Friedman, and A. A. Viggiano, J. Chem. Phys. **120**, 7024 (2004).

[8] S. Eden, P. Limão-Vieira, S. V. Hoffmann, and N. J. Mason, Chem. Phys. **323**, 313 (2006).

[9] F. Motte-Tollet, M.-J. Hubin-Franskin, and J. E. Collin, J. Chem. Phys. **97**, 7314 (1992).

[10] J. Delwiche, P. Natalis, J. Momigny, and J. E. Collin, J. Electron Spectrosc. Relat. Phenom. **1**, 219 (1972).

[11] L. Minnhagen, J. Opt. Soc. Am. **63**, 1185 (1973).

[12] J. H. D. Eland, *Photoelectron Spectroscopy* (Butterworths, London, 1994).

[13] L. Serrano-Andres and M. Merchan, J. Mol. Struct.: THEOCHEM **729**, 99 (2005).

[14] A. Dreuw and M. Head-Gordon, Chem. Rev. (Washington, D.C.) **105**, 4009 (2005).

[15] F. Aquilante, V. Barone, and B. O. Roos, J. Chem. Phys. **119**, 12323 (2003).

[16] C. Adamo and V. Barone, J. Chem. Phys. **110**, 6158 (1999).

[17] M. J. Frisch *et al.*, GAUSSIAN 03, Revision D.01. Gaussian, Inc., Wallingford, CT, 2004.

[18] O. Christiansen, H. Koch, and P. Jorgensen, Chem. Phys. Lett. **243**, 409 (1995).

[19] O. Christiansen, H. Koch, and P. Jorgensen, J. Chem. Phys. **105**, 1451 (1996).

[20] DALTON, a molecular electronic structure program, Release 2.0 (2005), see http://www.kjemi.uio.no/software/dalton/dalton.html

[21] K. Kaufmann, W. Baumeister, and M. Jungen, J. Phys. B **22**, 2223 (1998).

[22] P. J. Knowles, C. Hampel, and H.-J. Werner, J. Chem. Phys. **99**, 5219 (1993).

[23] J. D. Watts, J. Gauss, and R. J. Bartlett, J. Chem. Phys. **98**, 8718 (1993).

[24] P. G. Szalay and R. J. Bartlett, Chem. Phys. Lett. **214**, 481 (1993).

[25] MOLPRO, a package of *ab initio* programs designed by H.-J. Werner and P. J. Knowles, Version 2002.1, R. D. Amos *et al.*

[26] G. Schaftenaar and J. H. Noordik, J. Comput.-Aided Mol. Des. **14**, 123 (2000).

[27] G. Fisher, R. L. Purchase, and D. M. Smith, J. Mol. Struct. **405**, 159 (1997).

[28] C. Mao, C. Nie, and Z. Zhu, Spectrochim. Acta, Part A **27**, 1093 (1998).

[29] G. K. Jarvis, K. J. Boyle, C. Mayhew, and R. P. Tuckett, J. Phys. Chem. A **102**, 3230 (1998).

[30] M. A. Parkes, S. Ali, R. P. Tuckettt, V. A. Mikhailov, and C. A.

Mayhew, Phys. Chem. Chem. Phys. **8**, 3643 (2006).

[31] P. Limão-Vieira, S. Eden, P. A. Kendall, N. J. Mason, and S. V. Hoffmann, Chem. Phys. Lett. **364**, 535 (2002).

[32] Evaluation number 12, NASA, Jet Propulsion Laboratory, JPL Publication 97-4, 1997 (unpublished).

[33] E. Vasekova, E. A. Drage, K. M. Smith, and N. J. Mason, J. Quant. Spectrosc. Radiat. Transf. **102**, 418 (2006).

[34] C. H. Chang, R. F. Porter, and S. H. Bauer, J. Mol. Struct. **7**, 89 (1971).